Unusual nonlinear strain dependence of valence-band splitting in ZnO

Yelong Wu, Guangde Chen, Su-Huai Wei, Mowafak Al-Jassim, and Yanfa Yan

Phys. Rev. B **86**, 155205 — Published 8 October 2012

DOI: 10.1103/PhysRevB.86.155205

Unusual nonlinear strain dependence of valance-band splitting in ZnO

Yelong Wu,[1,2,3,*] Guangde Chen,[1] Su-Huai Wei,[2] Mowafak Al-Jassim,[2] and Yanfa Yan[3]

[1]*MOE Key Laboratory for Nonequilibrium Synthesis and Modulation of Condensed Matter, Xi'an Jiaotong University, Xi'an, Shaanxi 710049, China*

[2]*National Renewable Energy Laboratory, Golden, Colorado 80401, USA*

[3]*Department of Physics and Astronomy, The University of Toledo, Toledo, Ohio 43606, USA*

Abstract

Using first-principles band structure calculations, we investigate the crystal-field splitting and spin-orbit splitting at the valance band edge of ZnO, and their dependence on the strain. Different from other conventional semiconductors, the variation of the valance-band splitting of ZnO shows a strong nonlinear dependence on the strain and the slope of the crystal-field splitting as a function of strain can even change sign. Our analysis shows that this unusual behavior in ZnO is due to the strong coupling between Zn 3*d* states and oxygen 2*p* states. A mapping of the valence-band ordering in ZnO under different strain levels is provided which will be useful in designing ZnO based optoelectronic devices.

PACS numbers: 71.70.-d, 71.70.Fk, 71.15.Mb, 71.20.Nr

Strain can significantly modify the electronic band structures of a material [1–3], thus it can have strong effects on the structural, electrical and optical properties of the material [4–6]. Because of this, it has been extensive studied both theoretically and experimentally in the past decades and has often been used in designing electronic devices to enhance the device performance. There are many different ways to apply strain, e.g., by applying external stress, having lattice and/or crystal structure mismatch between the epi-film and substrate [4] or between the layers in a heterostructure superlattice [7], or having reconstructions on a polar surface [8].

ZnO has great potential for optoelectronic applications such as blue and ultra violet light sources [9, 10], transparent electrodes in electronic circuits [11], and solar cells [12]. Recently, there were some attempts to tailor the electrical and optical properties of ZnO through strain [13, 14]. Surprisingly, despite extensive experimental and theoretical study on this material, the dependence of the valence band splitting on the strain for ZnO has not been clearly analyzed yet. The knowledge of the electronic structure properties of ZnO is far from satisfactory, e.g., the size and sign of the crystal-field (Δ_{CF}) and spin-orbit (Δ_{SO}) split at the valence band maximum (VBM), which determine the order of the VBM states [$\Gamma_{9(6)v}$, $\Gamma_{7(6)v}$ and $\Gamma_{7(1)v}$, where the numbers in the parentheses of the subscript are the single group representations, i.e., in the absence of spin-orbit coupling] has been a long standing controversy for more than 50 years (see, e.g., Ref. [15] and references therein).

For most conventional tetrahedral bonded semiconductors, the lowest state of the conduction band minimum (CBM) is *s*-like, whereas the upmost states of the valence-band are mainly anion *p*-like. Therefore, for these materials such as AlN, the band splitting follows the behavior for *p* states and the electronic states shift almost linearly under strain which can be described by the deformation potentials *b* or *d* [16]. Consequently, the splittings, i.e. the energy level difference between the VBM states, induced by the intra-band deformation potentials change quasi linearly as functions of strain [17, 18]. However, in tetrahedral (T_d) symmetry the cation *d* and anion *p* states have the same symmetry representation, so they can couple to each other [19]. When the *p-d* coupling become large in some of the materials such as ZnO, the change of the VBM splitting as a function of strain could be very different than the conventional *sp* semiconductors.

Here, using first principles band structure calculation, we investigated the electronic band structure of ZnO, especially the crystal-field splitting and spin-orbit splitting at the Γ point valance band edge as functions of strain. We show that the variation of the valance-band splitting of ZnO with strain is very different from other conventional semiconductor, i.e., it shows a strong nonlinear

variations and the slope of the crystal-field splitting as a function of strain can even change sign. After analyzing the structural and electronic properties of ZnO under different strain condition, we concluded that it is the strong *p*-*d* coupling in ZnO that induces this abnormal behavior in the valance-band splitting of ZnO.

In our study, all the structural optimizations and energy band calculations are performed using the density-functional theory in the generalized-gradient approximation (GGA) [20]. The projected augmented wave method (PAW) [21] as implemented in the VASP (Refs. [22] and [23]) code is employed. The energy cutoff is set at 450 eV and an $8 \times 8 \times 8$ k-point grid is used for structural optimizations. All structures are fully relaxed until the force acting on each atom is less than 0.02 eV/Å.

In this letter, we focus on two types of strains which are the most commonly used in experiments: (1) uniaxial strain applied in the c-axis direction; (2) biaxial strain, i.e., epitaxial strain. For the uniaxial strain case, we fix the lattice constant c at different values, whereas the lattice constant a and the internal cell parameter u are allowed to relax. In this case, strain is defined as $\epsilon_1 = \epsilon_{zz} = (c - c_0)/c_0$. In the case of biaxial strain, a is fixed at several values and the c and u parameters are allowed to relax. The strain is then defined as $\epsilon_2 = \epsilon_{xx} = \epsilon_{yy} = (a - a_0)/a_0$. Here, a_0 and c_0 are the theoretical equilibrium lattice constants for the unstrained structure.

Figure 1 shows the crystal-field splitting and spin-orbit splitting at the top of valence-band in ZnO (triangle lines) under different biaxial and uniaxial strain levels. The crystal-field splitting parameters Δ_{CF} are calculated in the absence of spin-orbit interaction, $\Delta_{CF} = E(\Gamma_{6v}) - E(\Gamma_{1v})$. The spin-orbit splitting parameters Δ_{SO} are obtained by fitting the calculated top three energy levels at Γ to the quasi-cubic model of Hopfield [24] [with the center of the bands shifted by $(\Delta_{SO} + \Delta_{CF})/6$]

$$\begin{aligned} E(\Gamma_{9(6)v}) &= 1/2(\Delta_{SO} + \Delta_{CF}) \\ E(\Gamma_{7(1,6)v}) &= \pm 1/2[(\Delta_{SO} + \Delta_{CF})^2 - 8/3\Delta_{SO}\Delta_{CF}]^{1/2} \, . \end{aligned} \tag{1}$$

We can see that at equilibrium Δ_{CF} is positive and Δ_{SO} is negative in the GGA calculation, indicating the order of the valence band is $\Gamma_{7(6)v}$, $\Gamma_{9(6)v}$, $\Gamma_{7(1)v}$, in decreasing energy. We first look at the case of the system under uniaxial strain condition. From Figure 1, we can see that when we have tensile strain, both Δ_{CF} and Δ_{SO} increase as the strain increases. These results are expected because for most *sp* semiconductors, the Δ_{CF} increases with the c/a ratio. However, the situation becomes unusual when compressive uniaxial strain is applied. The change of the Δ_{CF} becomes slower and even changes sign and Δ_{CF} is always positive no matter how large the strain is. This abnormal behavior is totally different from other more conventional materials such as AlN which

has the same wurtzite structure as for ZnO, see Fig. 1. Because the obvious difference between these two kinds of materials in their electronic structures, i.e. the different positions of the cation *d* orbitals (Al 3*d* is *extravalence states*, whereas Zn 3*d* is *subvalence states*), we may attribute these phenomena to the *p*-*d* hybridization at the valance-band edge which are permitted in tetrahedron environment, see Fig. 2. *p*-*d* coupling (through a matrix element V_{pd}) mixes *d* character into the wave function at the VBM, and makes some difference in energy to the states. One can estimate the magnitude of these effects as $\Delta E_{pd} \sim V_{pd}^2/(\varepsilon_p^a - \varepsilon_d^c)$, in which $\varepsilon_p^a - \varepsilon_d^c$ means the state-energy difference, indicating that the *p*-like states at the edge of the valence-band have different strength of *p*-*d* coupling, i.e. different *d* component (e.g. Γ_{6v} is a pure *p*-*d* hybridized state but Γ_{1v} has mixed in some *s* orbitals, and strain may redistribute the *d* component in the relative states), and hence affect the splitting energies. The negative Δ_{SO} also can be attributed to the large *d* orbital component at the top of the valence band, since *d* states contribute with opposite sign to the spin-orbit splitting (lowering it), as opposed to *p* orbitals (which raise it) [19]. The increase of the volume reduces the *p*-*d* coupling at the VBM as the strain increasing, which explains why the Δ_{SO} becomes less negative. Similar but opposite trend is also observed when biaxial strain is applied. In this case, even the Δ_{SO} is nonlinear under tensile strain. The opposite behavior of biaxial vs. uniaxial strain can be understood by noticing that ZnO has positive Poisson ratio, i.e., in the compressive biaxial strain case, there is an elastic expansion of the lattice perpendicular to the strain direction, so c/a increases, whereas for in-plane tensile strain the c/a decrease, opposite to the uniaxial strain case. The relationship between the strain along and perpendicular to the *c* direction is $\epsilon_{zz} = -R^B\epsilon_2$ with $R^B = 2C_{12}/C_{33}$ [18]. For simplicity and representative, in most parts of this letter we just present the results of uniaxial strain case.

Because our calculated GGA values of Δ_{CF} and Δ_{SO} for equilibrium ZnO are 77 meV and -36 meV respectively, are much larger than the experimental results (41.7 meV and -8.0 meV) [25], one may question whether the density functional theory (DFT) is able to describe this phenomena correctly because it is known that DFT places the Zn 3*d* band at a too high energy, thus overestimates the *p*-*d* hybridization and incorrectly describe the splitting at the VBM. To test this, we use the so called LDA+*U* method [26] to adjust the position of the Zn 3*d* energy levels to be close to experimental values. Following Solovyev [27] and Laskowski [28] we use a spherically symmetric formulation of the LDA+*U* approach and used the effective $U_{eff} = U - J = 7.8$ eV. The crystal-field splitting and spin-orbit splitting energies of ZnO as functions of U_{eff} as well as the density of states resulting from the LDA+*U* calculations are presented in Figure 3. We find

that both the magnitudes of crystal-field Δ_{CF} and spin-orbit splitting Δ_{SO} decrease monotonically and nearly linearly as a function of increasing U_{eff}, i.e., decreasing in Zn 3*d* orbital energy. For U_{eff} = 7.8 eV, The calculated results Δ_{CF} = 31 meV and $\Delta_{SO} = -13$ meV are in good agreement with the experimental values. The results can be easily understood by noticing that for wurtzite structure the Γ_{6v} is a pure *p*-*d* hybridized state but Γ_{1v} has mixed in some *s* orbitals, so the *p*-*d* coupling for the Γ_{6v} state is larger than the Γ_{1v} state. Therefore, when *p*-*d* coupling decreases with increasing U_{eff}, the crystal field splitting $\Delta_{CF} = E(\Gamma_{6v}) - E(\Gamma_{1v})$ also decreases. Reducing *p*-*d* coupling also reduces the *d* component at the VBM, so the spin-orbit coupling also becomes less negative. These analysis are consistent with the calculated density of states showing that at U_{eff} = 7.8 eV the *d* character in the VBM states is considerably reduced as compared to the pure GGA calculations and the Zn 3*d* peak has moved down in energy with an average position of about -7 eV, which agrees with the experimental value of about -6.95 eV [29]. These results indicate that using LDA+*U* method would significantly improve the accuracy of the calculations of valence-band splitting, so in the following analysis, all the results are obtained from the LDA+*U* method.

Using the LDA+*U* approach, we calculated again the crystal-field splitting and spin-orbit splitting of the ZnO under different uniaxial and biaxial strain conditions (only uniaxial case is shown in Figure 1). We find that the general trend is the same as in the GGA calculation, i.e., the nonlinear variations still exist in the valence-band splitting as the strain varies. As a function of strain, the crystal-field splitting now can be negative under some large strain conditions. However, for any reasonable U_{eff} parameter, at zero strain, the crystal field splitting is always positive and the spin-orbit splitting is always negative because the *p*-*d* coupling in this system is significant and the positive contribution of the spin-orbit coupling due to oxygen *p* orbital is very small [19]. Therefore, the band order at the VBM should be $\Gamma_{7(6)v}$, $\Gamma_{9(6)v}$, $\Gamma_{7(1)v}$, in decreasing energy, in agreement with experiment results [25].

To unveil the underlying physics and understand more about these nonlinear variations of the valence-band splitting in ZnO, we examined the crystal-field splitting and spin-orbit splitting as functions of the structural parameters: volume (V), $\eta = c/a$ ratio, and the internal structure parameter u independently (u specifies the bond length $d_1 = uc$ along the c axis, see the inset in Fig. 4(a)), as the structure of the wurtzite is defined by these parameters. Figures 4(a)-(c) show the three structure parameters V, η and u as functions of uniaxial strain. We see that both V and ratio η decrease when the strain is more compressive. It is interesting to see that u parameter increases

under compressive strain. This is because to reduce the internal strain, the system tends to preserve the bond length. Therefore, when the c parameter decreases, to preserve the bond length, the u parameter will increase. In general, the structural parameters show the normal behavior of linear dependence under strain.

Figures 4(d)-(f) give the crystal-field and spin-orbit splitting energies vs. V, η and u respectively. It is clear that the crystal-field splitting is very sensitive to the change of η, while the spin-orbit splitting is mainly influenced by the change of u. The dependence of the Δ_{CF} and Δ_{SO} show the quasi linear dependence as a function of V or η. When V decreases, the increased p-d coupling enhances the Δ_{CF} but make the Δ_{SO} more negative, as discussed earlier. This is partially canceled by the p-p coupling between the oxygen $2p$ and Zn $4p$ orbitals. When η increases with fixed V and u, the Coulomb potential induced splitting on the p orbital makes Δ_{CF} increase. In this case, the bond length along the c direction is larger than the bond lengths away from the c direction, so the reduced p-d coupling in the c direction and increased p-d coupling away from the c direction also make the Δ_{CF} increase. The additive nature is the origin why Δ_{CF} is sensitive to the change of η. Because there are three bonds away from the c direction, whereas only one bond along the c direction, the spin-orbit splitting Δ_{SO} decreases as η increases. Contrary to the dependence on V and η, we find that for ZnO, the crystal field splitting Δ_{CF} has a strong non-liner dependence on u. The slope changes sign at a critical point u_c and the curve is almost quadratic. This is because when u increases at fixed V and η, the bond length along the c direction increases and the bonds away from the c direction decreases. Therefore, both p-p and p-d coupling decreases along the c direction [associated with the $E(\Gamma_{1v})$] but increases away from the c direction [associated with the $E(\Gamma_{6v})$]. However, the effect of p-p and p-d coupling is opposite. For most conventional semiconductor, p-p coupling is dominant, so Δ_{CF} will decrease as u increases, but for ZnO with large p-d coupling, for large u, Δ_{CF} increases. The Δ_{SO} decreases with u again because there are more bonds away from the c direction than along the c direction. Combine the changes of the structural parameters and the dependence of the Δ_{CF} and Δ_{SO} on the structural parameters, we can explain the results observed in Fig. 1.

Our discussion above suggest that the nonlinear variation of crystal-field splitting Δ_{CF} with the strain can be attributed to the change of internal structure parameter u, namely, internal strain due to a competition between the p-p and p-d coupling caused by the structural change. To further confirm this, we analyze the characters of partial charges at Zn muffin-tin site of the Γ_{6v} and Γ_{1v} states (Table I). When u increases, the bond lengths d_1 (axial bond) prolongs and d_2

(nonaxial bond) shrinks [inset in Fig. 4(a)]. As a result, the *p-d* coupling in the *xy*-plane would be strengthened, while in the *z* direction becomes weaker. For Γ_{6v} states, the total *p-d* coupling is getting stronger as *u* increasing (Table I, $d_{xy} + d_{x^2-y^2}$ increases, $d_{xz} + d_{yz}$ decreases and the total of them increases). This is consistent with our above analysis.

Finally, Figure 5 shows the valence-band ordering of ZnO under different levels of uniaxial strain calculated with LDA+U. It shows that, at strain free condition, the upmost state possesses Γ_7 symmetry resulting in a level ordering $\Gamma_{7(6)v}$, $\Gamma_{9(6)v}$ and $\Gamma_{7(1)v}$, which is in agreement with most of theoretical calculations and experimental results. A band crossing mainly caused by crystal-field splitting will occur at a certain compressive strain, with a consequence of the change of the valence-band ordering from $\Gamma_{7(6)v} - \Gamma_{9(6)v} - \Gamma_{7(1)v}$ to $\Gamma_{7(1)v} - \Gamma_{7(6)v} - \Gamma_{9(6)v}$. In addition, for not too large strains, such as in our calculations from -8% to 8%, the $\Gamma_{7(6)v}$ state is always above the $\Gamma_{9(6)v}$ state due to the negative spin-orbit splitting.

We have examined several other Zn chalcogenides, such as ZnS, ZnSe and ZnTe, and obtained similar results. However, as the *p-d* reduces as the anion size increases, the nonlinear relationship in the valence-band splitting of the zinc chalcogenides also diminishes.

In summary, we have investigated the valence-band splitting of ZnO and its strain dependance using first-principle calculation. We found that due to large *p-d* coupling in ZnO, it exhibits unusual behavior, i.e., the variations in valance-band splitting vs. strain is strong nonlinear. Based on our theoretical study, we presented the valence-band ordering in ZnO under different strain conditions. The mechanism and the underlying physics unveiled in the present work provided new insights on the understanding of semiconductor band structures and should be very useful in applying strain to enhance the device performance by modifying the band structures in designing electronic and optical devices.

Y. Wu and G. Chen gratefully acknowledge the financial support of the China National Natural Science Fund (Grant Nos. 11074200 and 61176079). Y. Yan acknowledges the support from the Ohio Research Scholar Program (ORSP). The work at NREL is supported by the U.S. Department of Energy under Grant No. DE-AC36-08GO28308.

* yelong.wu@stu.xjtu.edu.cn

[1] S. Thompson, G. Sun, Y. S. Choi, and T. Nishida, IEEE Trans. Electron Devices **53**, 1010 (2006).

[2] K. H. Hong, J. Kim, S. H. Lee, and J. K. Shin, Nano Lett. **8**, 1335 (2008).

[3] Y. Wu, G. Chen, S.-H. Wei, M. M. Al-Jassim, and Y. Yan, Appl. Phys. Lett. **99**, 262103 (2011).

[4] R. Ghosh, D. Basak, and S. Fujihara, J. Appl. Phys. **96**, 2689 (2004).

[5] A. J. Kulkarni, M. Zhou, K. Sarasamak, and S. Limpijumnong, Phys. Rev. Lett. **97**, 105502 (2006).

[6] A. Janotti, D. Segev, and C. G. Van de Walle, Phys. Rev. B **74**, 045202 (2006).

[7] Q. X. Yu, B. Xu, Q. H. Wu, Y. Liao, G. Z. Wang, R. C. Fang, H. Y. Lee, and C. T. Lee, Appl. Phys. Lett. **83**, 4713 (2003).

[8] S. H. Park, S. Y. Seo, S. H. Kim, and S. W. Han, Appl. Phys. Lett. **88**, 251903 (2006).

[9] D.C. and Look, Mater. Sci. Eng. B **80**, 383 (2001).

[10] A. Tsukazaki, A. Ohtomo, T. Onuma, M. Ohtani, T. Makino, M. Sumiya, K. Ohtani, S. F. Chichibu, S. Fuke, Y. Segawa, H. Ohno, H. Koinuma, and M. Kawasaki, Nat. Mater. **4**, 42 (2005).

[11] G. Hirata, J. McKittrick, T. Cheeks, J. Siqueiros, J. Diaz, O. Contreras, and O. Lopez, Thin Solid Films **288**, 29 (1996).

[12] M. Martínez, J. Herrero, and M. Gutiérrez, Sol. Energy Mater. Sol. Cells **45**, 75 (1997).

[13] A. Schleife, C. Rodl, F. Fuchs, J. Furthmuller, and F. Bechstedt, Appl. Phys. Lett. **91**, 241915 (2007).

[14] L. Kou, C. Li, Z.-Y. Zhang, C. Chen, and W. Guo, Appl. Phys. Lett. **97**, 053104 (2010).

[15] W. R. L. Lambrecht, A. V. Rodina, S. Limpijumnong, B. Segall, and B. K. Meyer, Phys. Rev. B **65**, 075207 (2002).

[16] A. Blacha, H. Presting, and M. Cardona, Phys. Status Solidi B **126**, 11 (1984).

[17] S.-H. Wei and A. Zunger, Phys. Rev. B **49**, 14337 (1994).

[18] J.-M. Wagner and F. Bechstedt, Phys. Rev. B **66**, 115202 (2002).

[19] S.-H. Wei and A. Zunger, Phys. Rev. B **37**, 8958 (1988).

[20] J. P. Perdew and Y. Wang, Phys. Rev. B **45**, 13244 (1992).

[21] P. E. Blöchl, Phys. Rev. B **50**, 17953 (1994).

[22] G. Kresse and J. Furthmüller, Comput. Mater. Sci. **6**, 15 (1996).

[23] G. Kresse and J. Furthmüller, Phys. Rev. B **54**, 11169 (1996).

[24] J. J. Hopfield, J. Phys. Chem. Solids **15**, 97 (1960).

[25] M. Fiebig, D. Frhlich, and C. Pahlke-Lerch, physica status solidi (b) **177**, 187 (1993).

[26] V. I. Anisimov, J. Zaanen, and O. K. Andersen, Phys. Rev. B **44**, 943 (1991).

[27] I. Solovyev, N. Hamada, and K. Terakura, Phys. Rev. B **53**, 7158 (1996).

[28] R. Laskowski and N. E. Christensen, Phys. Rev. B **73**, 045201 (2006).

[29] R. Girard, O. Tjernberg, G. Chiaia, S. Sderholm, U. Karlsson, C. Wigren, H. Nyln, and I. Lindau, Surf. Sci. **373**, 409 (1997).

TABLE I. The projected wavefunction characters of the Γ_{6v} and Γ_{1v} states (electron numbers) at the Zn site.

band	u	$p_x + p_y$	p_z	$d_{xy} + d_{x^2-y^2}$	$d_{xz} + d_{yz}$	d_{z^2}
Γ_{6v}	0.356	0.012	0.000	0.108	0.080	0.000
	0.368	0.016	0.000	0.124	0.071	0.000
	0.379	0.022	0.000	0.140	0.061	0.000
	0.390	0.028	0.000	0.158	0.053	0.000
	0.402	0.034	0.000	0.175	0.044	0.000
Γ_{1v}	0.356	0.000	0.046	0.000	0.000	0.215
	0.368	0.000	0.032	0.000	0.000	0.201
	0.379	0.000	0.020	0.000	0.000	0.184
	0.390	0.000	0.010	0.000	0.000	0.164
	0.402	0.000	0.004	0.000	0.000	0.141

FIG. 1. (Color online) Crystal-field splitting (Δ_{CF}) and spin-orbit splitting (Δ_{SO}) energies of ZnO and AlN under uniaxial (ϵ_1) and biaxial (ϵ_2) strain conditions as functions of the strains, calculated using GGA and LDA+U with U_{eff}=7.8 eV.

FIG. 2. (Color online) Schematic plot of valance-band splitting in wurtzite semiconductors, (a) without d and (b) with d. Δ_{cf}^{0} denotes the crystal field splitting induced by Coulomb potential. Δ_{pp} and Δ_{pd} represent the contributions from p-p coupling and p-d coupling, respectively.

FIG. 3. (Color online) (a) Crystal-field splitting (Δ_{CF}) and spin-orbit splitting (Δ_{SO}) energies of ZnO as functions of U_{eff}; (b) Density of states (DOS) of ZnO calculated with GGA and LDA+U. The energy of the VBM is set to be zero.

FIG. 4. (Color online) (a)-(c) The volume V, ratio $\eta = c/a$, and the internal structure parameter u as functions of uniaxial strain; (d)-(f) Crystal-field splitting (Δ_{CF}) and spin-orbit splitting (Δ_{SO}) as functions of V, η, and u, independently, i.e., (d) V varies, η and u are fixed at 1.633 and 0.375, respectively; (e) η varies, u is fixed at 0.375 and V is fixed at the value of strain free case, V_0; (f) u varies, η is fixed at 1.633 and V is fixed at V_0.

FIG. 5. (Color online) The valence-band ordering of ZnO under different levels of uniaxial strain. The energies of $\Gamma_{7(6)v}$-band are set to be zero.

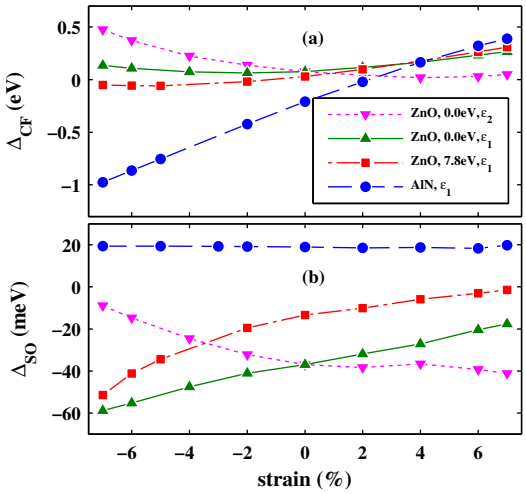

Figure 1 29Jun2012

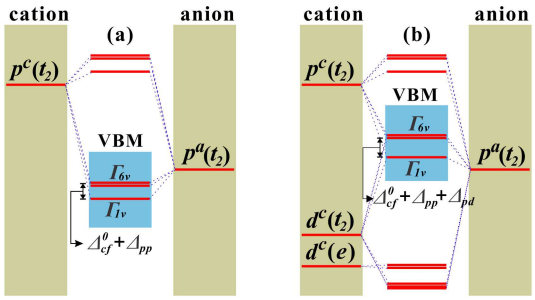

Figure 2 29Jun2012

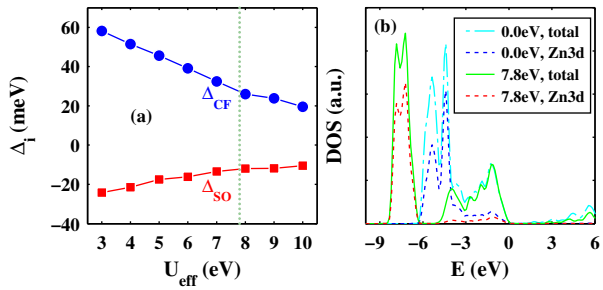

Figure 3 29Jun2012

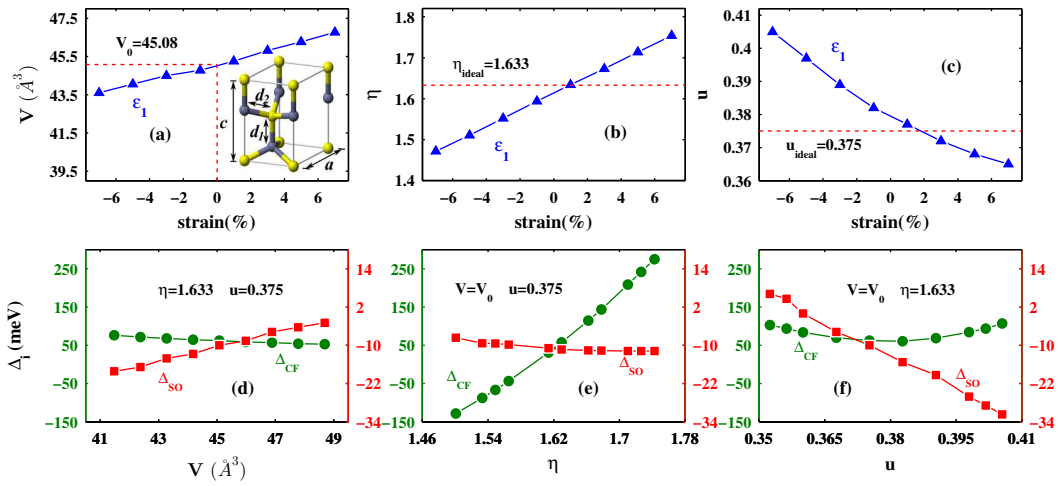

Figure 4 29Jun2012

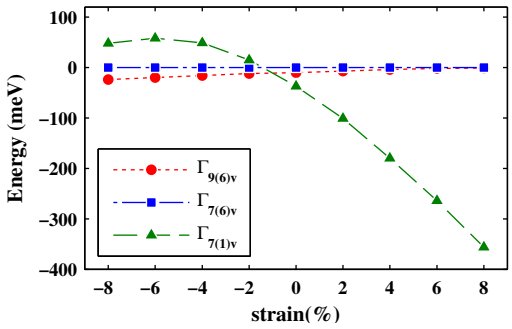

Figure 5 29Jun2012